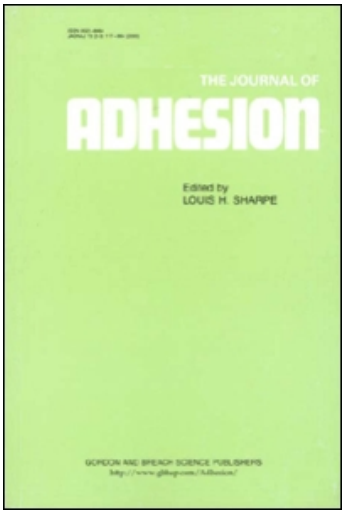

The Journal of Adhesion
Publication details, including instructions for authors and subscription information:
http://www.informaworld.com/smpp/title~content=t713453635

Photoelastic Studies on Rubber-to-Rubber Joints

Amalendu Sarkar[a]; Anil K. Bhowmick[a]; Swapan Majumdar[b]
[a] Rubber Technology Centre, Indian Institute of Technology, Kharagpur, INDIA [b] Department of Civil Engineering, Indian Institute of Technology, Kharagpur, INDIA

To cite this Article Sarkar, Amalendu , Bhowmick, Anil K. and Majumdar, Swapan(1991) 'Photoelastic Studies on Rubber-to-Rubber Joints', The Journal of Adhesion, 36: 2, 161 — 175
To link to this Article: DOI: 10.1080/00218469108027070
URL: http://dx.doi.org/10.1080/00218469108027070

J. Adhesion, 1991, Vol. 36, pp. 161–175
Reprints available directly from the publisher
Photocopying permitted by license only

Printed in the United Kingdom

Photoelastic Studies on Rubber-to-Rubber Joints

AMALENDU SARKAR, ANIL K. BHOWMICK

Rubber Technology Centre, Indian Institute of Technology, Kharagpur-721 302, INDIA

SWAPAN MAJUMDAR

Department of Civil Engineering, Indian Institute of Technology, Kharagpur-721 302, INDIA

(Received November 27, 1990; in final form July 19, 1991)

Photoelasticity is a method which yields information on the principal stress difference and orientation in a composite structure. Various problems associated with this technique, especially those concerning the fundamental relationship between the fringe order and the stress, have yet to be investigated. A few studies of this relationship in a universal stress state have been presented, particularly in the field of rubber-to-metal and rubber-to-fabric composites, but no evaluations have so far been made in the field of rubber-to-rubber joints. Applying the photoelastic method, we report our observations on the stress distribution in a natural rubber to natural rubber joint subjected to uniaxial tension. A comparison between the results of experimental photoelastic studies and the corresponding computer modelling has been illustrated. The theoretical displacement pattern of the angular joints of bi-rubber part has also been highlighted.

KEY WORDS photoelasticity; finite element analysis (FEA); joint; composite; adhesion; computer modelling; natural rubber.

INTRODUCTION

The experimental determination of the magnitude and distribution of stress within a body is extremely important to design a safe, simple or complicated composite structure. In the past such knowledge has been often drawn from practical experience. Most stress-analysis techniques are based on direct linear stress-strain measurements which are less accurate when the body being studied exhibits non-linear stress-strain and viscoelastic behaviour. Attempts have been made to design suitable stressmeters to analyse the stress within the model composite, but in the field of rubber-rubber two component specimens there has been limited success due to the complexity of the problem. In the case of rubber-rubber joints, contact stresses and stress distributions across the bondline are involved when the two parts of different stiffnesses are bonded together. This is found in many common practical applications such as tires, belts, hoses, etc. In such cases, the two-dimensional

photoelastic stress analysis appears to be one of the most suitable methods for obtaining a complete analysis of the problem.

In our earlier communications,[1,2] we have investigated the stresses, strains and strain energy densities of rubber-rubber joints based on the numerical method of finite element analysis (FEA). Lindley[3,4] has studied the deformation problems of a single rubber matrix from the viewpoint of plane stress and plane strain by FEA techniques. Seki *et al.*[5] have applied the FEA for multilayer rubber-to-metal composite bearings which undergo large elastomeric deformation. Gent and Kaang[6] have qualitatively used photoelasticity to monitor the progress of debonding in rubber-to-metal joints under compression. Ridha and Crano[7] have performed photoelastic studies to evaluate the stress distributions in the three most common cord-adhesion tests—ASTM D2229-80, MICA and TCAT and observed that the results of such analyses are in good agreement with the computer results. Analytical methods, however powerful, may need experimental verification. In this regard, a detailed experimental investigation has also been conducted by the authors[8] to study the fracture behaviour of rubber-to-rubber joints and the effects of joint angle on fatigue life. Two-dimensional photoelasticity may offer the most suitable way of correlating the experimental observations with the theoretical understanding.

Emphasis in this paper is placed on photoelastic models to study the stress distributions in rubber-to-rubber joints. Photoelastic and finite element stress analyses (FEA) are employed to generate the fringes in computer modelling. Finally, theoretical predictions are compared with the experimental observations. To simplify the problem, the actual geometry is taken into consideration. Photoelastic analysis is conducted on a thin rubber-rubber, two-component specimen where the Y-dimension is quite large. Equivalent moduli for plane-stress test specimens loaded in tension are compared for the theoretical and experimental analysis. In order to make this comparison possible and meaningful, the following assumptions are made in the theoretical development:

1) The composite geometry is perfect and regular.
2) The two-component part has no initial defect or flaw.
3) The two-component material as a whole is macroscopically homogeneous.

However, to avoid errors associated with the mechanical properties of the materials and loading arrangements, natural rubber based transparent gum and opaque filled systems have been used for the two-component material in photoelastic analysis. The calibration has also been conducted on the single transparent gum material. The details of the calibration procedure are discussed in the literature.[9,10]

THEORY

For a continuous, incompressible, hyperelastic, homogeneous and isotropic material, the Mooney-Rivlin[11] strain energy density function "W" can be expressed as,

$$W = W(I_i(\lambda_i(E_{ij}))) \tag{1}$$

where, I_i ($i = 1, 2, 3$) are the principal strain invariants, λ_i ($i = 1, 2, 3$) the principal extension ratios and E_{ij} the strain tensors. Since rubber deforms incompres-

sively, $\lambda_1\lambda_2\lambda_3 = 1$. According to the Green-Lagrange tensor analysis[12] for a largely deformed finite strain component, the strain is related to the principal extension ratio as,

$$\lambda_1^2 = 1 + 2\,E_{11} \tag{2a}$$

$$\lambda_2^2 = 1 + 2\,E_{22} \tag{2b}$$

For a homogeneous plane stress deformation the principal stresses σ_1 and σ_2 are derived from "W" as [13]

$$\sigma_1 = 2\left(\lambda_1^2 - \frac{1}{\lambda_1^2\lambda_2^2}\right)\left(\frac{\partial W}{\partial I_1} + \lambda_2^2\frac{\partial W}{\partial I_2}\right) \tag{3a}$$

$$\sigma_2 = 2\left(\lambda_2^2 - \frac{1}{\lambda_1^2\lambda_2^2}\right)\left(\frac{\partial W}{\partial I_1} + \lambda_1^2\frac{\partial W}{\partial I_2}\right) \tag{3b}$$

The first order partial derivatives of the strain energy function $\partial W/\partial I_1$ and $\partial W/\partial I_2$ of the Mooney-Rivlin form cannot be determined analytically. They can only be determined experimentally. On simplification, for a deformed isotropic, incompressible elastic material, the principal true stresses σ_1 and σ_2 are related to the strain components as

$$\{\sigma\} = [D]\{E\} \tag{4}$$

where,

$$[D] = \begin{bmatrix} D_{11} & D_{12} & 0 \\ D_{21} & D_{22} & 0 \\ 0 & 0 & \dfrac{D_{11}\,D_{22}}{(D_{11}\,D_{22})^{1/2} + 2D_{12}} \end{bmatrix} \tag{5}$$

[D] represents a property matrix which depends upon the elastic strain and the material constants $\partial W/\partial I_1$ and $\partial W/\partial I_2$.

$$D_{11} = \left\{8\left(\frac{\partial W}{\partial I_1} + \frac{\partial W}{\partial I_2}\right)(1 + E_{11}) + 16\left(\frac{\partial W}{\partial I_1} + 2\frac{\partial W}{\partial I_2}\right)(E_{22} + E_{11}E_{22}) + 8\left(\frac{\partial W}{\partial I_2}\right)\left(\frac{E_{22}^2}{E_{11}} + E_{11}E_{22}^2\right)\right\}/(1 + 2E_{11})(1 + 2E_{22}) \tag{5a}$$

$$D_{12} = D_{21} = \left\{4\left(\frac{\partial W}{\partial I_1} + \frac{\partial W}{\partial I_2}\right) + 32\left(\frac{\partial W}{\partial I_2}\right)(E_{11}E_{22})\right\}/(1 + 2E_{11})(1 + 2E_{22}) \tag{5b}$$

$$D_{22} = \left\{8\left(\frac{\partial W}{\partial I_1} + \frac{\partial W}{\partial I_2}\right)(1 + E_{22}) + 16\left(\frac{\partial W}{\partial I_1} + 2\frac{\partial W}{\partial I_2}\right)(E_{11} + E_{11}E_{22}) + 8\left(\frac{\partial W}{\partial I_2}\right)\left(\frac{E_{11}^2}{E_{22}} + E_{11}^2E_{22}\right)\right\}/(1 + 2E_{11})(1 + 2E_{22}) \tag{5c}$$

In order to express stress in terms of an arbitrary x-y coordinate system, it is only necessary to employ the equations governing the transformation of tensors of the second order in two dimensions used commonly in mechanics of materials (Mohr's

circle).[14] Finally, fringe order in each element is computed from the principal stress differences and the computer model is generated in a graphics terminal (on a color monitor).

EXPERIMENTAL DETAILS

In the photoelastic experiment, the model two-component specimen consists of softer and birefringent material "A" (gum natural rubber), and opaque and stiffer material "B" (filled natural rubber). Figure 1 shows a model specimen which is representative of the type of rubber-rubber joints used in our experiment.

Fabrication of the Two-Component Specimen

The formulations of the mixes are given in Table I. The test specimens have been prepared in two stages. In the first stage, a uniform uncured sheet has been prepared between two thin aluminium sheets under light pressure (2 MPa) in the mould for a very short period of time at 100°C. The aluminium sheets have then been removed from both sides of the sheet. In the second stage, two halves of dissimilar materials of uniform thickness have been joined together under controlled pressure. The optimum cure time (12.5 mins.), temperature (150°C) and pressure (5 MPa) of the uncured rubber compound have been employed. The dimensions of the test pieces

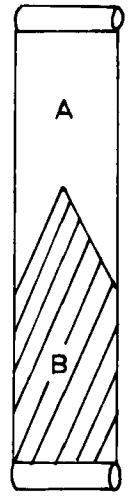

A MODEL RUBBER-RUBBER
TWO-COMPONENT PATTERN

FIGURE 1 A model rubber-rubber two-component specimen.

TABLE I
Formulation of the birefringent and opaque material

	I	II
NR	100	100
ZnO	5	—
Stearic acid	2.5	—
HAF[a]	50	—
CBS[b]	0.6	—
S	2.5	—
DCP[c]	—	1.0
Small strain		
Modulus, MPa (100% elongation)	1.53	0.50
Stress optical coefficient, $Pa^{-1} \times 10^9$	—	1.92

[a]HAF—High abrasion furnace black, supplied by Phillips Carbon Black Ltd., Durgapur, INDIA.
[b]CBS—Cyclohexyl benzthiazyl sulphenamide, supplied by ICI, Rishra, Hooghly, INDIA.
[c]DCP—Dicumyl peroxide, supplied by Hercules Inc., Wilmington, USA.

are given in Figure 2. The extensional modulus of the individual components has been determined as per ASTM D412–80 in a Zwick UTM 1445 from the initial slope of the stress-strain curve.

Photoelastic Analysis of the Model Bi-Rubber Part

Photoelastic studies have been made to evaluate whole-field information about the stress distributions in the rubber-rubber joints. The conventional photoelastic method uses a model of transparent macromolecular material to deal with the elastic stress-strain problems. In this experiment, full scale samples have been prepared using natural rubber (NR) (the transparent and opaque materials having different stiffness) to eliminate any scaling error. It may be mentioned that NR gum vulcanizate is a photoelastic model material.[15] The birefringence is produced when the rubber-rubber two-component specimen is stretched (in a specially prepared grip) in the field of a plane polariscope (model no. ASIR-30, research type) in between the polariser and the analyser. A sketch of the attachments (RCG, Pune, India) is shown in Figure 3. A halogen lamp has been used as the monochromatic light source (wavelength ~5700 A. For the two-dimensional photoelastic analysis of an isotropic

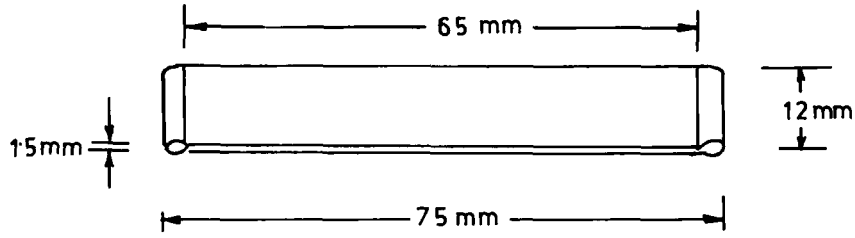

FIGURE 2 Dimensions of the test specimen.

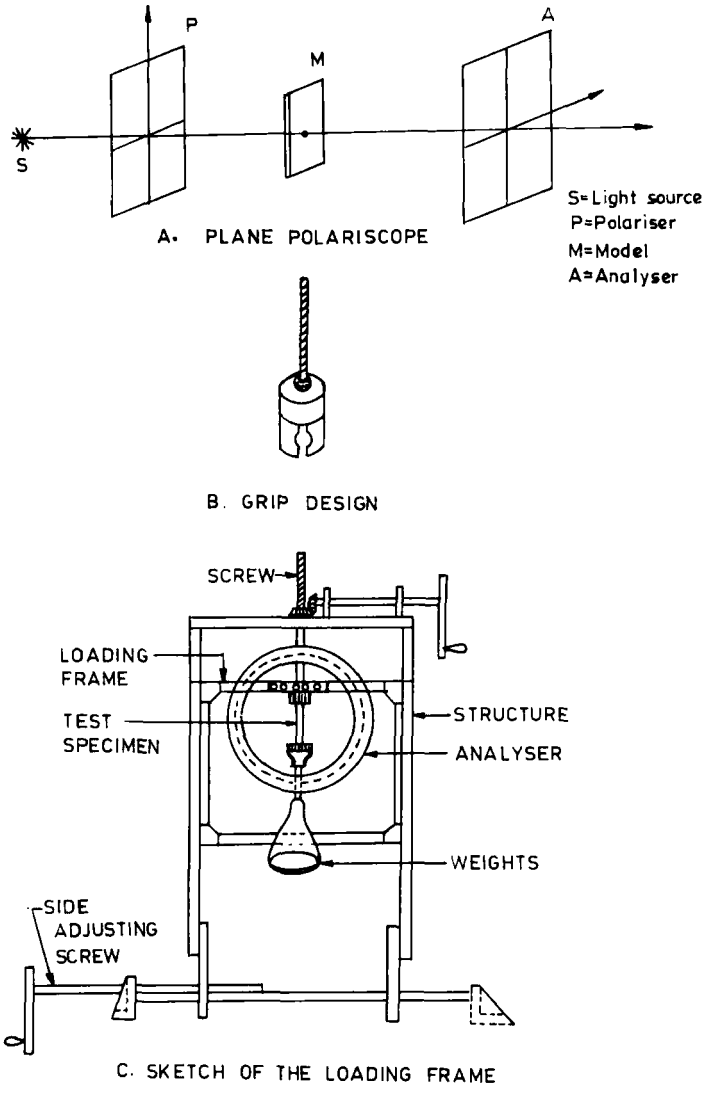

FIGURE 3 Sketch of the attachment in the polariscope. (A) Plane polariscope (B) Grip design and (C) Sketch of the loading frame showing Screw, Loading frame, Test specimen, Weight, Structure and Side adjusting screw, Analyser.

material, the maximum shear stress is proportional to half the principal stress difference. Along lines of uniform colour (isochromatics), the difference in the principal stresses is constant. The colour progression for increasing stress difference is yellow, red and green (the original study has been done using a white light source and colour photography). In the black and white photo reproductions, the number of fringes observed indicates the stress difference magnitude. All the experiments have been

carried out at a temperature of 25°C. More detailed descriptions of photoelasticity are available in the literature.[9,10]

Photography

The photographs of the isochromatic fringe patterns have been taken across the bondline of the angular rubber-rubber two-component joints using an Asahi Pentax Camera (model No. K1000).

Calibration of Single Rubber

In photoelastic analysis, the principal stress difference can be predicted if the material fringe value of the individual material is known. The stress conditions at different levels of loading can be found from isochromatic and isoclinic fringe patterns.

Calibration has been done by selecting a transparent birefringent body (based on natural rubber in our case) for which the theoretical stress distribution is accurately known. The specimen has been loaded uniaxially in the monochromatic light field and fringes have been generated successively with the gradual increment of loading. The uniaxial stress is determined by the equation

$$\sigma_1 = \frac{P}{h.b} \tag{6}$$

$$\sigma_2 = 0$$

$$\sigma_3 = 0$$

where "h" is the thickness of the specimen, "b" the width of the specimen, "P" the load applied and σ_i (i = 1, 2, 3) the principal stresses.

The isochromatic material fringe value "f_σ" is calculated based on the equation

$$f_\sigma = \frac{(\sigma_1 - \sigma_2)h}{N} \tag{7}$$

or,

$$f_\sigma = \frac{P}{b.N} \tag{8}$$

where "f_σ" is the material fringe value and "N" the fringe order.

It is clear that the material fringe value is independent of thickness of the material. Knowing the fringe order and corresponding load, the material fringe value can be found easily. In our experiment we have plotted the fringe order against the stress as shown in Figure 4. The fringe order "N" follows a linear relationship with stress. In the computer program, local fringe value is computed on the basis of the stress-fringe order relationship.

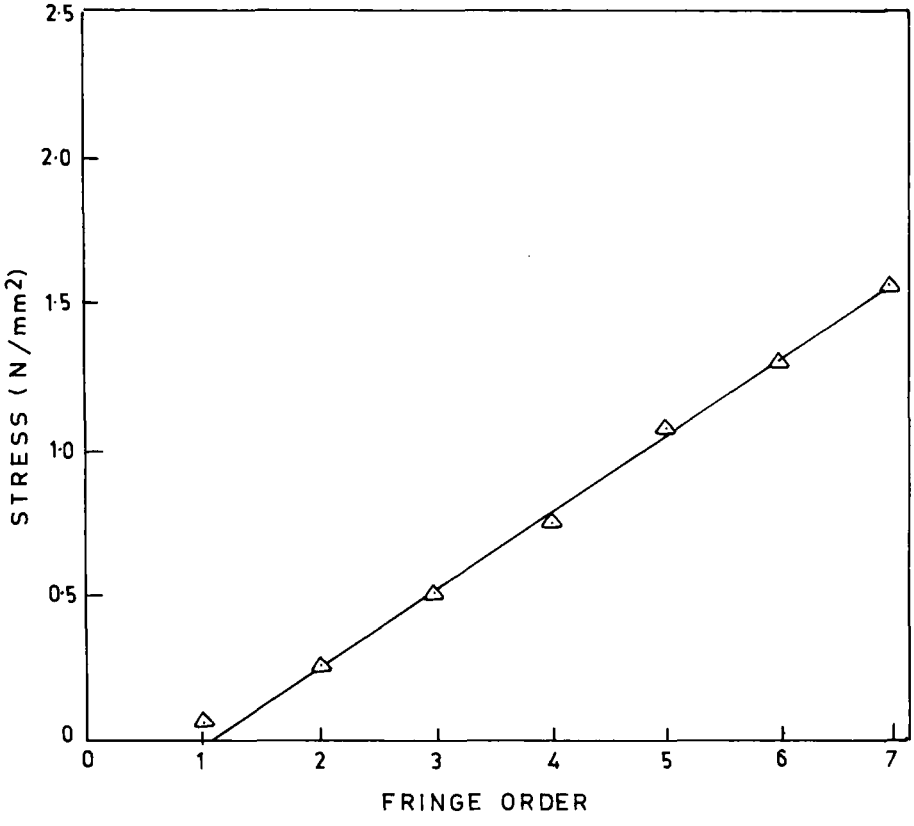

FIGURE 4 Calibration curve of transparent birefringent material. Stress *vs.* fringe order.

RESULTS AND DISCUSSION

To understand the stress distribution and the mechanism of fracture, an investigation has been conducted by preparing simple rubber-rubber joints. Two types of bi-rubber specimens have been studied as shown in Figure 5. The only difference between the two-component specimens—type I and type II—is that the materials are interchanged. The isochromatic fringe patterns, as obtained at different load levels in a monochromatic light field, are shown in Figures 6(a), 6(b) and 6(c) for two component specimen type I, while Figures 7(a), 7(b) and 7(c) show the same for specimen type II. In the black and white photo reproductions, symmetric fringe patterns are observed in both types of model composite specimens which demonstrate the actual stress gradient at different levels of loading. From Figures 6(a)–7(c) it is noted that the fringe patterns are generated at different zones depending upon the geometry of the two-component joint and the stress. For the type I specimen, the fringes are generated at the angle tip and travel towards the edges of the

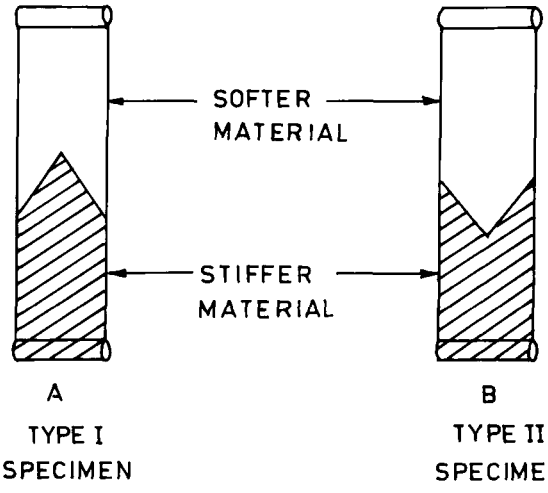

FIGURE 5 Two types of bipart specimens (A) Specimen type I; (B) Specimen type II.

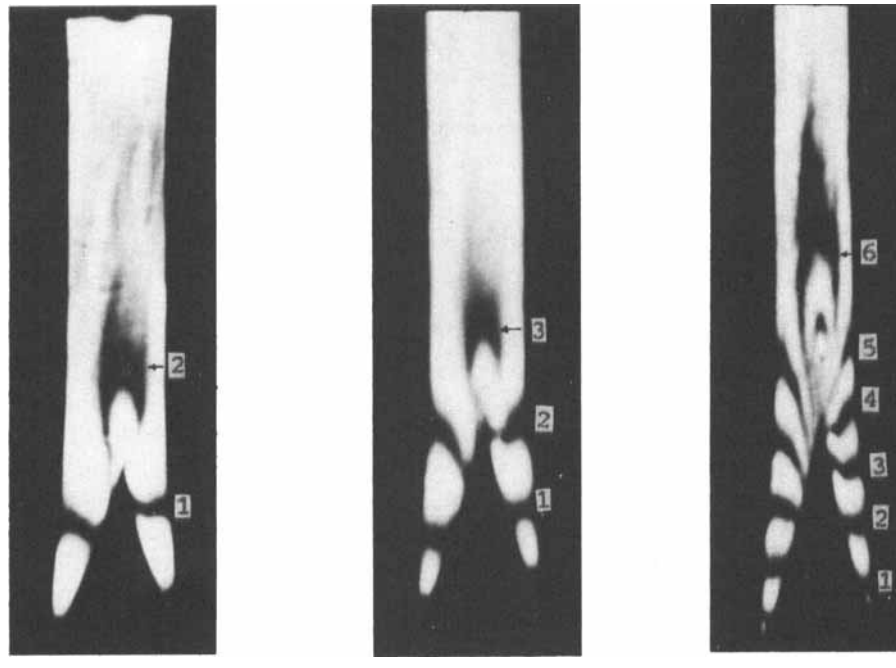

(a) (b) (c)

FIGURE 6 Isochromatic fringe patterns of two-component specimen type I at different loading conditions: (a) 6.3N; (b) 9.25N; (c) 18.25N.

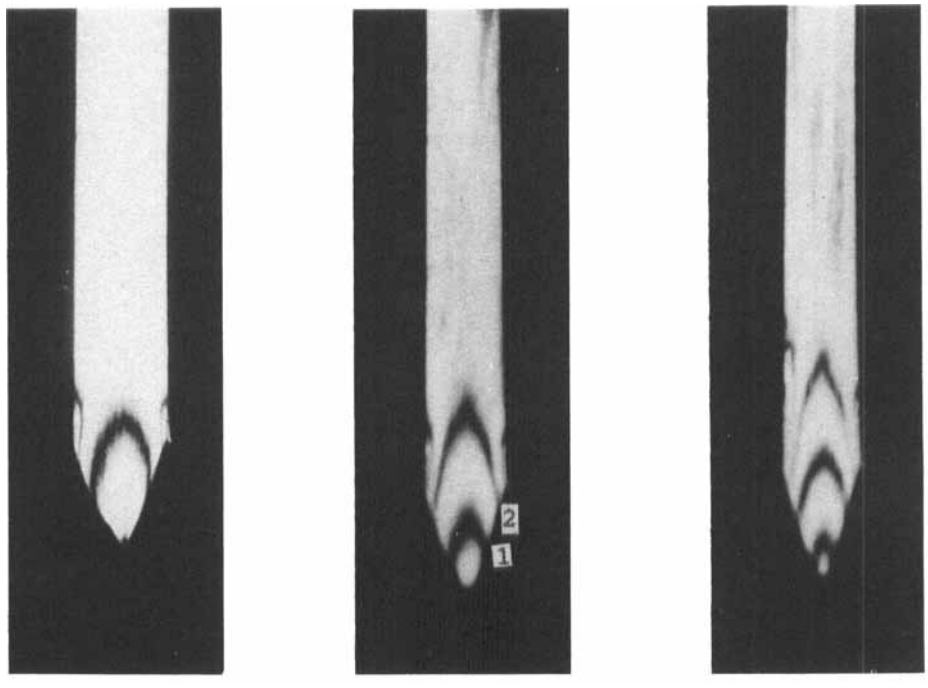

(a) (b) (c)

FIGURE 7 Isochromatic fringe patterns of two component specimen type II at different loading conditions: (a) 6.5N; (b) 9.75N; (c) 15.6N.

joint. This indicates the maximum stress concentration site at the angle tip. For the type II two-component specimen, however, the fringes appear near the edges of the joint and move towards the angle tip of the joint. The fringes are also numbered in order of their generation for type I and type II specimens as shown in the same photograph. Moreover, it is noted that there is a stress gradient at the angle tip for the type I specimen at all load levels—it is more severe at the higher load levels (~18N) [Figure 6(c)]. In this simple tensile test, the specimen is in a state of uniaxial stress since the Poisson's ratio mismatch between the layers is small. The distribution of the difference of principal stresses, "$\Delta\sigma$", in the overall two-component specimen under loading is calculated using the fringe order obtained in the photoelastic experiment. Photographs of the fringe patterns are also taken in the white light field as shown in Figures 8(a)–8(c) for two component specimen type I and Figures 9(a)–9(c) for specimen type II. Yellow, red and green bands are the indication of the relative stress differences.

Another noticeable feature is that the generation of fringes in the two-component specimen (across the bondline) is much faster as compared with that of the single birefringent material at any particular incremental level of loading.

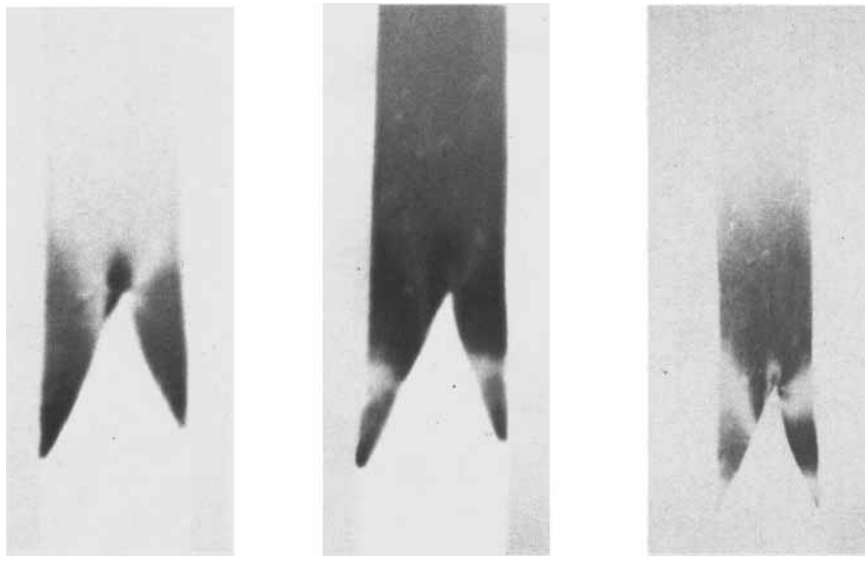

(a) (b) (c)

FIGURE 8 Photograph of the fringe pattern of two-component specimen type I in white light field: (a) 6.3N; (b) 9.2N; (c) 18.25N. See Color Plate I.

Theoretical Calculation and a Comparative Study with Experimental Findings

Attempts have also been made to simulate the photoelastic behaviour of the rubber-rubber joints using the finite element analysis (FEA). For this purpose, a software program, as discussed earlier, has been developed for the case of large-deformation, non-linear mechanics in order to calculate normal stresses (σ_x, σ_y) and shear stress (Γ_{xy}). The FEA also gives the information about the principal stresses (σ_1 and σ_2) in each element. This principal stress can be separated from the fringe order information. This is often preferred because it needs no experimental information other than boundary values of stress. When this computer program is executed in a graphics terminal, a contour map as shown in Figure 10 is obtained from equation 7. For the convenience of the analysis, calculation for the theoretical model has been carried out for the half section of the two-component specimen across the bondline. To compare the actual fringe pattern in a rubber-rubber two-component specimen, the type I specimen as shown in photograph 6(b) is chosen. It is evident that the theoretical model predicting the fringe patterns and displacement patterns matches qualitatively with the experimental observations. The theoretical displacement pattern across the bondline of the angular rubber-rubber joints for two-component type I and type II specimens are shown in Figure 11. It is observed that the theoretical displacement pattern is in qualitative agreement with the experi-

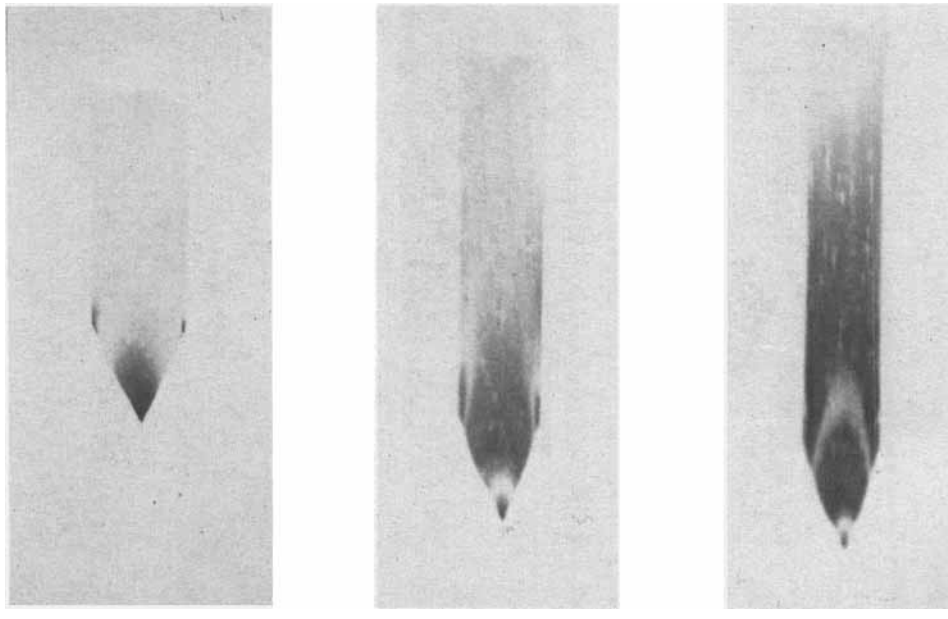

(a) (b) (c)

FIGURE 9 Photographs of the fringe patterns of two-component specimen type II in white light field: (a) 6.33N (b) 9.75N; (c) 15.6N. See Color Plate II.

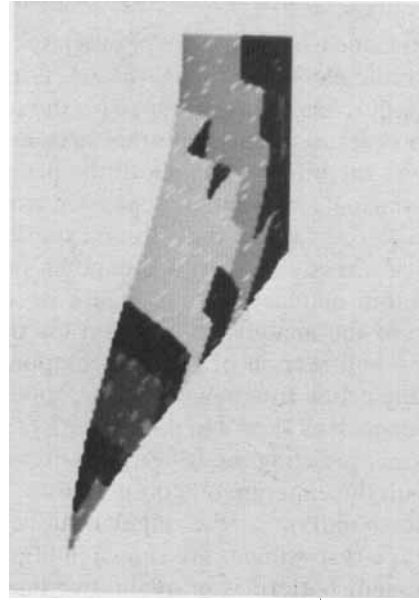

FIGURE 10 Theoretical photoelastic model of the fringe patterns of the rubber-rubber joint. See Color Plate III.

mental displacement pattern at the same level of loading (*cf.* Figures 6(b) and 7(b) with Figure 11). At any particular level of load, it is also observed that the displacement vector has a much higher magnitude for material of lower stiffness as compared with stiffer material system in the binary rubber-rubber joints. In the theoretical model (as generated in the graphics terminal), the different stress levels are indicated by different colour bands and the order is as follows:

$$\text{sky blue} > \text{pink} > \text{blue} > \text{yellow} > \text{green}.$$

Experimental Finding and its Mechanism

Figures 12(a) and 12(b) show the nature of fracture of two-component specimens—type I and type II. As shown in earlier figures, the stresses are high at the angle tip for the type I specimen and at the edges of the joint for the type II specimen. Experiments for the joints show that the failure of the type I structure nucleates near the angle tip while the fracture of type II structure starts at the edges. However, the initiation of fracture does not indicate the total fracture path. In such cases, the microfracture generally nucleates in the weaker material near the interface and the lack of constraint ahead of the crack tip allows the crack to propagate without much hindrance through the weaker phase. As a result, it is observed that, although the fracture initiates near the interface, propagation is nowhere near the interface.

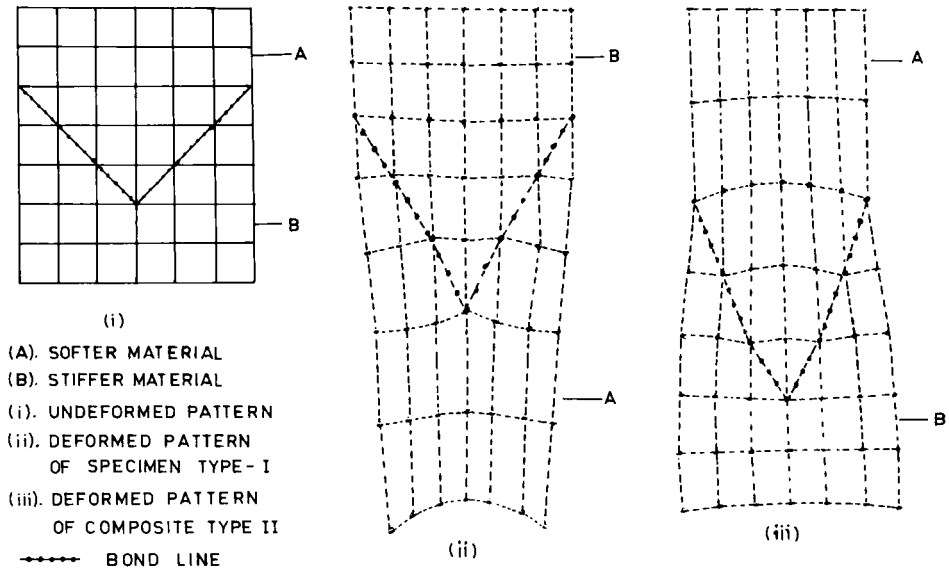

FIGURE 11 Theoretical displacement pattern of the two-component specimens—type I and type II.

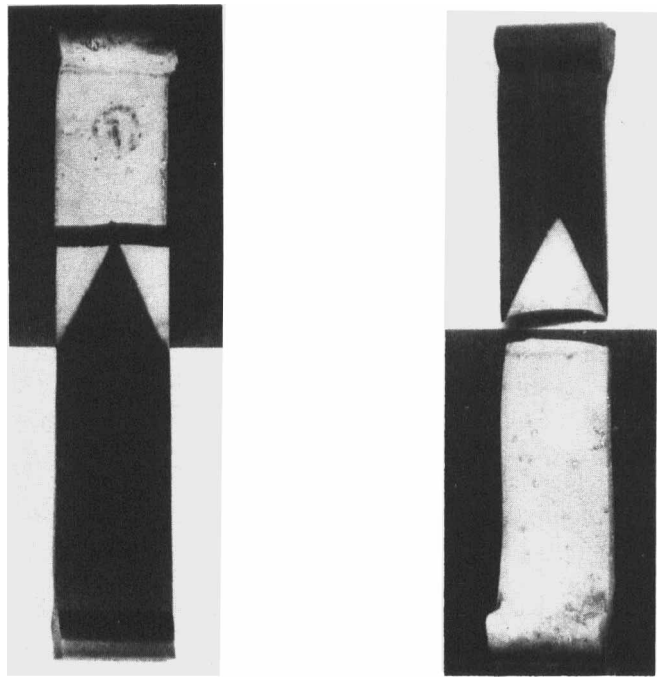

(a) (b)

FIGURE 12 Nature of fracture of (a) two component specimen type I and (b) two component specimen type II.

CONCLUSION

From the photoelastic experiment, it is clearly observed that the stress concentration is maximum near the angle tip for the type I joint and near the edges of the joints for the type II specimen. In actual practice, the phenomenon of fracture nucleation follows the same pattern in both cases. A software program based on the theory of photoelasticity has been developed and used to generate the fringe pattern in a computer model based on the data gathered from the numerical method of FEA. The theoretical model and the experimental fringe patterns and displacement patterns are qualitatively in accord with each other.

Acknowledgement

The authors are indebted to the M/S Neolac Rubber Mfg. Co. Pvt. Ltd., 16, DumDum Road, Calcutta—700016, India for necessary help.

References

1. A. Sarkar, D. Dutta, S. Majumdar and A. K. Bhowmick, *Plastics and Rubber Processing and Applications*, **14,** 49 (1990).
2. A. Sarkar, D. Dutta, S. Majumdar and A. K. Bhowmick *Rubber Chem. Technol.* (accepted for publication).
3. P. B. Lindley, *J. Strain Analysis*, **6,** 45 (1971).
4. P. B. Lindley, *J. Strain Analysis*, **10,** 25 (1975).
5. W. Seki, Y. Fukahori, Y. Isada, T. A. Matsunaga, *Rubber Chem. Technol.*, **60,** 856 (1987).
6. A. N. Gent and S. Y. Kaang, *Rubber Chem. Technol.*, **62,** 757 (1989).
7. R. A. Ridha and R. N. Crano, *Rubber Chem. Technol.*, **56,** 252 (1983).
8. A. Sarkar and A. K. Bhowmick, *J. Adhesion Sc. and Tech.* **5,** 389 (1991).
9. J. W. Dally and W. F. Riley, *Experimental Stress Analysis* (McGraw Hill Book Company, New York, 1978), pp. 143–250.
10. W. H. Tuppeny and A. S. Kobayshi, *Manual on Experimental Stress Analysis* (Westport, Connecticut, 1965).
11. R. S. Rivlin, "Forty years of non-linear continuum mechanics," *Proc. IX Intl. Congress on Rheology*, Mexico (1984).
12. Y. C. Fung, *Foundation of Solid Mechanics* (Prentice-Hall International Inc., United Kingdom, 19), pp. 434–456.
13. R. S. Rivlin and D. W. Saunders, *Phil. Trans. Roy, Soc.* **A243,** 251 (1951); *Trans. Faraday Soc.*, **48,** 200 (1952).
14. J. D. Walter, *Rubber Chem. Technol.*, **51,** 524 (1970).
15. L. R. G. Treloar, *The Physics of Rubber Elasticity*, 2nd Edition (Oxford University Press, London, 1967), Chap. 10.